Journal of Structural Biology 208 (2019) 115–126

Contents lists available at ScienceDirect

Journal of Structural Biology

journal homepage: www.elsevier.com/locate/yjsbi

# Reconstruction of plant microstructure using distance weighted tessellation algorithm optimized by virtual segmentation

Wangyu Liu[a,*], Ling Zhang[a], Jiale Huang[a,b], Weigui Xie[a]

[a] School of Mechanical and Automotive Engineering, South China University of Technology, Wushan Road, Tianhe District, Guangzhou 510641, People's Republic of China
[b] Department of Mechanical and Electrical Engineering, Xiamen University, Xiamen 361005, People's Republic of China

ARTICLE INFO

*Keywords:*
Tessellation
Geometry modelling
Plant microstructure
Reconstruction algorithm

ABSTRACT

The accurate reconstruction model of plant microstructure is important for obtaining the mechanical properties of plant tissues. In this paper, a virtual segmentation technique is proposed to optimize Delaunay triangulation. Based on the optimized Delaunay triangulation, an Optimized Distance Weighted Tessellation (ODWT) algorithm is developed. Two different structures, namely carrot and retting maize vascular bundles, were reconstructed via the ODWT algorithm. The accuracy of ODWT is evaluated statistically by comparing with Centroid-based Voronoi Tessellation (CVT) and Area Weighted Tessellation (AWT). The results show that ODWT has distinct advantages over CVT and AWT. It is worth mentioning that ODWT has better performance than CVT when there exists large diversity in adjacent cell area. It is found that CVT and AWT fail to reconstruct cells with elongated and concave shapes, while ODWT shows excellent feasibility and reliability. Furthermore, ODWT is capable of establishing finite tissue boundary, which CVT and AWT have failed to realize. The purpose of this work is to develop an algorithm with higher accuracy to implement the preprocessing for further numerical study of plants properties. The comparison results of the simulated values of the longitudinal tensile modulus with the experimental value show that ODWT algorithm can improve the prediction accuracy of multi-scale models on mechanical properties.

## 1. Introduction

The structures of plants and their tissues often exhibit excellent mechanical properties. Bionic design inspired by plant structures has stimulated the emergence of a large number of new technologies and structures (Saavedra Flores and Haldar, 2016; Malek et al., 2017). Natural plant tissues often exhibit very sophisticated multi-scale structural hierarchy, shown as Fig. 1. Obviously, the mechanical properties of wood at the macroscale (view 1 and view 2 from left to right) are decided by its sub-levels (view 3 to view 5 from left to right). Usually, the cell structure of plants is typical and representative (view 4 and view 5), and the mechanical behavior of various plant cells was widely investigated at the microscale (Liu et al., 2015; Malek and Gibson, 2017; Jin et al., 2015). As the mechanical behavior of plants at macroscale is largely influenced by moisture and temperature, it is very difficult to directly compute its mechanical properties (Liu et al., 2015; Wang et al., 2013). It is desirable to establish a multiscale model to make sure the properties could be transformed from microscale to macroscale. Therefore, a bridge must be built between macroscale and microscale, which makes the reconstruction of plants tissue (view 3) necessary. On the one hand, the model should have a superior accuracy for reconstruction of real morphology; on the other hand, the model should be simple enough to guarantee efficient calculations (Pieczywek et al., 2011).

The accurate establishment of mechanical models of plant tissue at various scales is of great significance for the study of plant mechanical properties. At the mesoscale, the model of the porous structure of plant is an important unit for bridging the macroscopic structure of plant and the microscopic structure of cell walls. Accurate reconstruction method for this complex porous structure model is particularly important. For the modeling of irregular porous structures of plants, the three-dimensional structure can be accurately reconstructed by CT scanning (Palombini et al., 2016). But such a model is too complicated for finite element calculation. Thus, it is more efficient to reconstruct the two-dimensional cross-section structure, which can be developed into three dimensions by stretching in the longitudinal direction. The Voronoi method based on Delaunay triangulation is a classical method for reconstructing irregular porous structures of plants (Faisal et al., 2013; Gibson, 2005; Ghosh et al., 1996). Mattea et al. (1989) applied the algorithm Voronoi tessellation to simulate the microstructure of fruit

* Corresponding author.
*E-mail address:* mewyliu@scut.edu.cn (W. Liu).

https://doi.org/10.1016/j.jsb.2019.08.008
Received 29 October 2018; Received in revised form 10 August 2019; Accepted 18 August 2019
Available online 19 August 2019

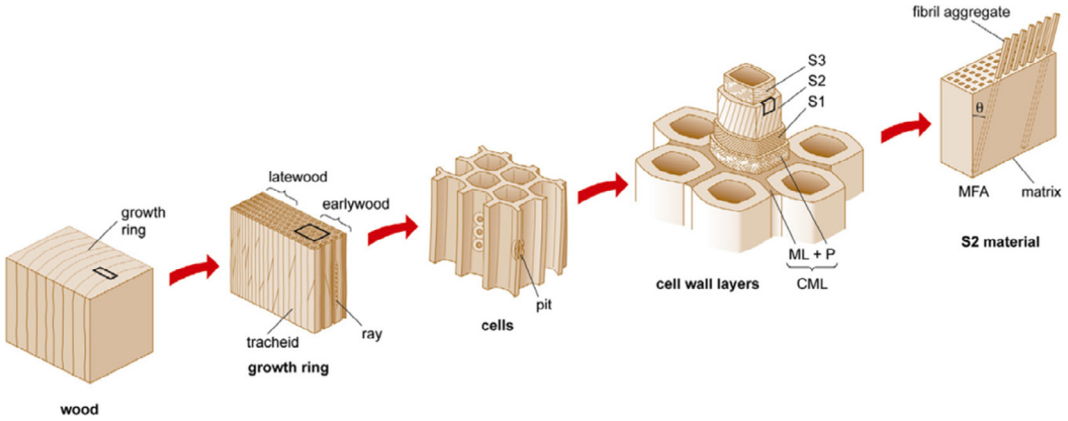


**Fig. 1.** Multi-scale structure of the wood. View 1 and view 2 research the mechanical properties of plants at the macroscale. In view 3, cell structure of plant tissue is reconstructed at the mesoscale. In the fourth and fifth views, the hierarchical structure and material composition of cell walls are studied in the micro and ultra-micro scales. The mechanical properties of wood at the macroscale (view 1 and view 2 from left to right) is decided by its sub-levels (view 3 to view 5 from left to right). The purpose of this work is to develop an accurate algorithm for modelling of the cell structure in the mesoscale (view 3). It is a necessary bridge between macroscale (view 1 and view 2) and microscale (view 4 and view 5). (From Rafsanjani et al. (2012)), with permission from Elsevier.)

tissue for the first time in studying the dehydration of fruit. Mebatsion et al. (2006a) used the Centroid-based Voronoi Diagram (CVD) and the Poisson Voronoi Diagram (PVD) to simulate the growing of different apple cultivars with 2D models, but the results showed that neither CVD nor PVD could achieve an accurate reconstruction of the apple tissues. Mebatsion et al. (2006b) developed an ellipse tessellation to reconstruct the 2D geometric model of apple tissues, which showed improved accuracy compared with Voronoi tessellation. However, the curve boundary is adverse to the subsequent finite element analysis (FEA). Besides, concave shape cells cannot be accurately reconstructed through this method. Ntenga and Beakou (2011) successfully reconstructed plant fiber cross-sections utilizing the Voronoi plugin in ImageJ. Because of the infinite boundary, Voronoi diagrams need to be processed before being imported into the FEA software. The Finite-Edge Centroid Voronoi Tessellation (FECVT) was developed to solve the problem of infinite boundaries generated in Voronoi diagrams (Faisal et al., 2012, 2014). But it is regrettable that the accuracy of traditional Voronoi tessellation still requires significant improvement. Wang et al. (2014) developed an area weighted tessellation (AWT) algorithm based on Delaunay triangulation to improve the accuracy of CVT when there is large difference in the neighboring cell area. However, when the adjacent cell area differs too much, or the cell shape is concave or extraordinarily slender, the reconstruction accuracy is unsatisfying. Huang et al. (2017) reconstructed the retting maize vascular bundles sections by skeletonization method with high accuracy. Nevertheless, too many boundary lines were generated through this method, resulting in calculation difficulties in the later FEA simulation.

Voronoi tessellation is also commonly used in the analysis of atomic structures and the cryo-electron microscopy. Luo and Samwer (2018) explored the atomic structure of metallic glass by scanning tunneling microscopy (STM), and established the structural model based on high resolution STM image, generating icosahedral order on the surface and different Voronoi clusters in 3-D space. Andronov et al. (2018) studied the 3D structure of cellular structures by Single-molecule localization microscopy, and developed 3D ClusterViSu based on 3D Voronoi tessellations to research the cellular structures.

The microscopic topological morphology of the cells of plant tissues varies greatly. For example, some cell structures are similar to convex polygons, but some others are concave or slim. Some plant tissues are relatively uniform, but some others have large size difference between adjacent cells. For many plant structures like vascular bundles, the size between adjacent cells is greatly different. Some images of the plant tissue used for structural analysis are difficult to be reconstructed due to the existence of finite boundaries. The diversity of plant structures makes it difficult to develop a general algorithm for accurate reconstruction of various structures. The main purpose of this paper is to explore a reconstruction algorithm oriented for a large scope of application and high accuracy, i.e., not only the above-mentioned models of various plant structures are covered, but also the accuracy of the topology requirement for further research of the mechanical properties are ensured. A Delaunay triangulation based on virtual segmented optimization is proposed for concave and slender cells, the target cells that influence the accuracy of reconstruction. Concerning the zone where the size of the adjacent cells differs greatly, an algorithm named Distance Weighted Tessellation (DWT) is proposed based on the AWT to facilitate more effective reconstruction. A method, namely the optimized distance weighted tessellation (ODWT), is developed for identifying and reconstructing the finite tissue boundaries. It is evaluated that this method could fulfill the task to build an integrated tissue boundary for those with or without the finite boundaries. Two completely different plant tissues, namely the carrot and retting maize vascular bundles, were used to verify the reconstruction effect, including the accuracy and efficiency of the algorithm. The results were verified by statistical analysis of the reconstructed images.

## 2. Materials and methods

The ODWT algorithm proposed in this paper operates on binary images. Therefore, the first step is to convert the microscopic images of plant tissues into binary images. The image is obtained using a Scanning Electron Microscope (SEM). Then, the coordinates of the cell centroid points and tissue boundary points can be obtained from the binary image, which will be used for the next step to carry out the Delaunay triangulation optimization by virtual segmentation. The last step is to reconstruct the image through the algorithm DWT based on the Delaunay triangulation (Lee and Schachter, 1980). The Delaunay triangulation is a special triangulation that the circumcircle of each triangle does not contain any other points in the point set. The last two steps are called as algorithm ODWT, which has great influence on the accuracy of reconstruction. Compared with current existing algorithms, ODWT could effectively optimize the last two steps and reconstruct the finite boundary for plant tissues. The algorithms are implemented by Matlab R2014a (The Math-Works, Inc., Natick, MA) with the following flowing chart (Fig. 2).

### 2.1. Image acquisition

In order to evaluate the algorithm's applicability adaptive to

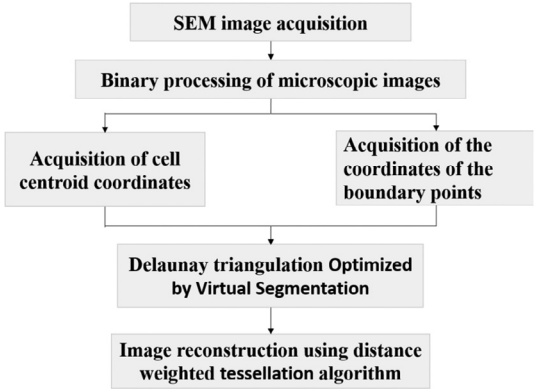


**Fig. 2.** The flowchart of ODWT algorithm for reconstructing plant tissues. The last two steps are the most important steps of the algorithm ODWT and have great influence on the accuracy of reconstruction.

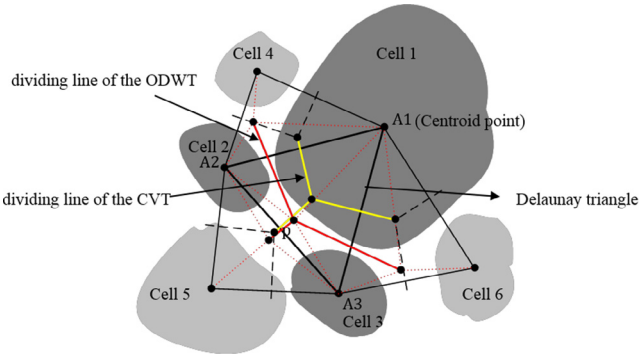


**Fig. 4.** The principle of DWT, the yellow line is the dividing line of the CVT, and the red line is the DWT dividing line. By using CVT, the small cells will be enlarged, and large cells will be shrunk. While ODWT provides an accurate reconstruction of the cells.

different plant tissues, as well as the reconstruction accuracy, two plant tissues with great variations, carrot and retting maize vascular bundles, were chosen in this study. In order to make the evaluation more convincing, both the plant tissue images and binary images are all originated from the published literatures (Huang et al., 2017; Pieczywek et al., 2011), shown as Fig. 3.

In order to make the context more easily understood by readers, we give a simple introduction to the sample preparation, both cited from the literatures mentioned above,

(1) The slices were obtained from fresh carrots and were stained in Coryphopshyne O. Then the slices of carrot tissue were observed by confocal scanning laser microscope and the microscopic image was taken (Zdunek and Umeda, 2005). The skeletons of the cellular structure (Fig. 3a) were obtained using Aphelion v.3.2 (Adcis, France) image analysis software (Pieczywek et al., 2011).
(2) The stems were collected from mature maize plants and were retted in a sealed container at room temperature for about 20 days. Therefore the fiber bundles of maize could be extracted from the stems by hand using water (Huang et al., 2016). The slices were taken from the fiber bundles and were sputter coated with a thin layer of gold. Then the samples were observed by SEM (Quanta 200, America) under accelerating voltage of 10 kV to capture the microscopic image. Lastly, the binary image of retting maize vascular bundle was obtained, as shown in Fig. 3c.

It could be observed from the figure that the carrot tissue shows great variations of cell size and shape in the same cross section. For example, there are either protoxylem vessel or metaxylem vessel nearby a particular cell, which brings big challenge to the accuracy of reconstruction algorithm. Moreover, some concave polygons formed by the dissolution of phloem tissue might also present in the cross section of retting maize vascular bundle. Regarding these two issues of plant tissues, a new algorithm must be investigated to promote the accuracy of tissue reconstruction. At the same time, the application scope could be enlarged.

### 2.2. Reconstruction of the cellular cross section

#### 2.2.1. Distance weighted tessellation

When cells are reconstructed with traditional CVT or FECVT, those cells with large differences with adjacent cells are difficult to be accurately reconstructed. The small cells will be enlarged, while the large cells will be shrunk. The algorithm AWT proposed by Wang et al. (2014) made a notable improvement in solving this problem. However, the accuracy of the AWT is still insufficient, because the small cells are likely to be annexed by surrounded large cells. Based on the Delaunay triangulation, we proposed an algorithm DWT (Fig. 4), which is originated from AWT but more adaptive to the problem. The algorithm can be described as the following steps,

(1) Extract the centroid points of the cells and perform Delaunay triangulation, the image is divided into a number of triangles with the cell centroids acting as the apexes of the triangles.
(2) Segment the Delaunay triangles, and mark the sides as the cell walls.
(3) Calculate the radius of the cells' equivalent circles, i.e., the circles that have the same area with the cells, and take it as the weighting factor to determine the apex of the cell walls.

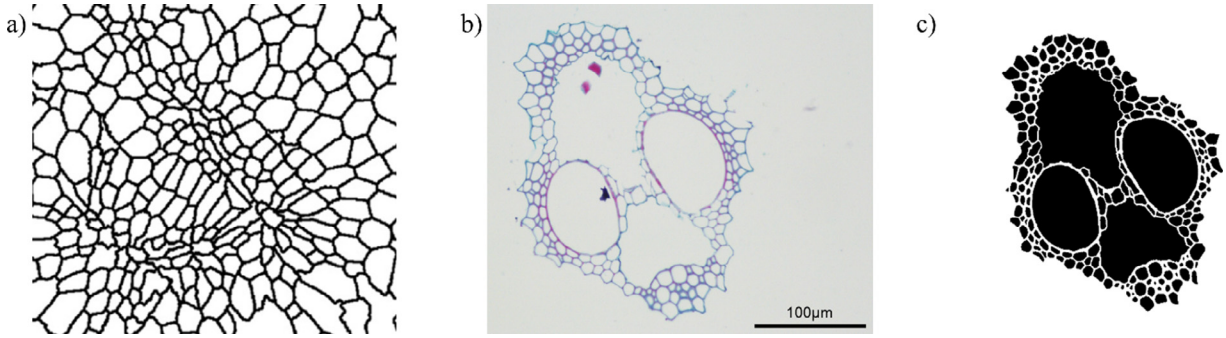


**Fig. 3.** (a) Binary image of carrot. It shows great variations of cell size and shape. (From Pieczywek et al. (2011), with permission from Elsevier.) (b) Microscopic picture of retting maize vascular bundle. There exist some large cavities adjacent to many small cells and concave polygons which are difficult to be reconstructed. (From Huang et al. (2017), with permission from Springer.) (c) Binary image of retting maize vascular bundle. The algorithm ODWT proposed in this paper is operated on binary images. (From Huang et al. (2017), with permission from Springer.)

The third step makes the DWT distinct from CVT, FECVT and AWT. The CVT and FECVT take the center of the circumscribed circle of each Delaunay triangle as the apex of the cell walls. The AWT uses the area of the cells where the vertices of the Delaunay triangle are located as the weighting factor to determine the apex of the cell wall. Distinguishingly, DWT uses the radius of the cells' equivalent circles as the weighting factor to determine the apex of the cell walls.

Now an example is given to show the detail process of the algorithm. In Fig. 4, triangle $A_1A_2A_3$ is a Delaunay triangle obtained by connecting the centroids of three adjacent cells. $A_1$, $A_2$ and $A_3$ are the centroids of three adjacent cells, and P is the apex of the cell wall that DWT needs to determine. Three lines of $A_1P$, $A_2P$ and $A_3P$ divide the triangle into three parts. The areas of the three sub-triangles will be assigned with the weight factor. Since the bottom edges ($A_1A_2$, $A_2A_3$ and $A_3A_1$) of the three sub-triangles are known, only the distance from P to the three bottom edges, i.e., $r_1$, $r_2$, $r_3$, are required to be used to represent the radius of the equivalent circles of the cells in which $A_1$, $A_2$ and $A_3$ are located. Supposing $S_1$, $S_2$ and $S_3$ are the areas of cells. Then the following formula is obtained,

$$r_1 : r_2 : r_3 = \sqrt{S}_1 : \sqrt{S}_2 : \sqrt{S}_3 \tag{1}$$

The Distance weight factor is determined by:

$$Z_{ij} = r_i + r_j \quad (i \neq j\&i,\ j = 1, 2, 3) \tag{2}$$

The area of the sub-triangle $A_iA_jP$ is calculated by:

$$S_{ij} = \frac{Z_{ij}}{Z_{12} + Z_{13} + Z_{23}} * S \quad (i \neq j\&i,\ j = 1, 2, 3) \tag{3}$$

where S is the area of Delaunay triangle $A_1A_2A_3$. The coordinates of $A_1$, $A_2$ and $A_3$ are known in advance through step 1 and step 2. Suppose the coordinates of $A_1$ is represented by $(x_i, y_i)$, then the value of S can be obtained through the following formula,

$$S = \mathrm{abs}\left(\frac{1}{2}\begin{vmatrix} x_1 & y_1 & 1 \\ x_2 & y_2 & 1 \\ x_3 & y_3 & 1 \end{vmatrix}\right) \tag{4}$$

According to the formulas (1)–(3) and the coordinates of $A_1$, $A_2$ and $A_3$, there is only one solution to the coordinate of point P, which can be determined by resolving the above formulas. Now the algorithm DWT is completed, and it can be implemented by connecting the apex of the cell wall in three Delaunay triangles that are adjacent to triangle $A_1A_2A_3$.

### 2.2.2. Virtual segmentation of cell area

When the microscopic images of plant tissues are reconstructed, CVT, AWT and DWT are all based on Delaunay triangulation by taking the centroid of the cell cavity as the apex. Any Delaunay triangle does not contain the centroids of other cells. In the process of Delaunay triangulation, the triangles are formed with three nearest points. Therefore, when the area of the cell cavity is concave or has large eccentricity, it is difficult to identify all the neighboring cells of the cell cavity. Fig. 5 shows the flowchart of DWT-based Delaunay triangulation. $P_0$ is the centroid point of the elongated cell 1, and those from cell 2 to cell 8 are the adjacent cells of cell 1. The centroid points of all cells are firstly extracted, shown as Fig. 5a. Delaunay triangulation is performed with these centroid points, as shown in Fig. 5b. The cyan lines are the edges of Delaunay triangle. The centroid point of cell 2 or cell 5 is not the apex of the same triangle with the centroid point of cell 1. The reconstructed structure obtained by DWT-based Delaunay triangulation is shown in Fig. 5c. The reconstructed cell 1 is neither adjacent to cell 2 nor to cell 5, therefore the reconstructed cell 1 is severely distorted.

Therefore the Delaunay triangulation should be optimized to make sure that cell 1 can share the Delaunay triangle with all adjacent cells (cell 2–8). Fig. 6 shows the flowchart of the DWT-based virtual segmentation (ODWT). The so-called virtual segmentation is actually an optimization of Delaunay triangulation, which can be divided into the following steps.

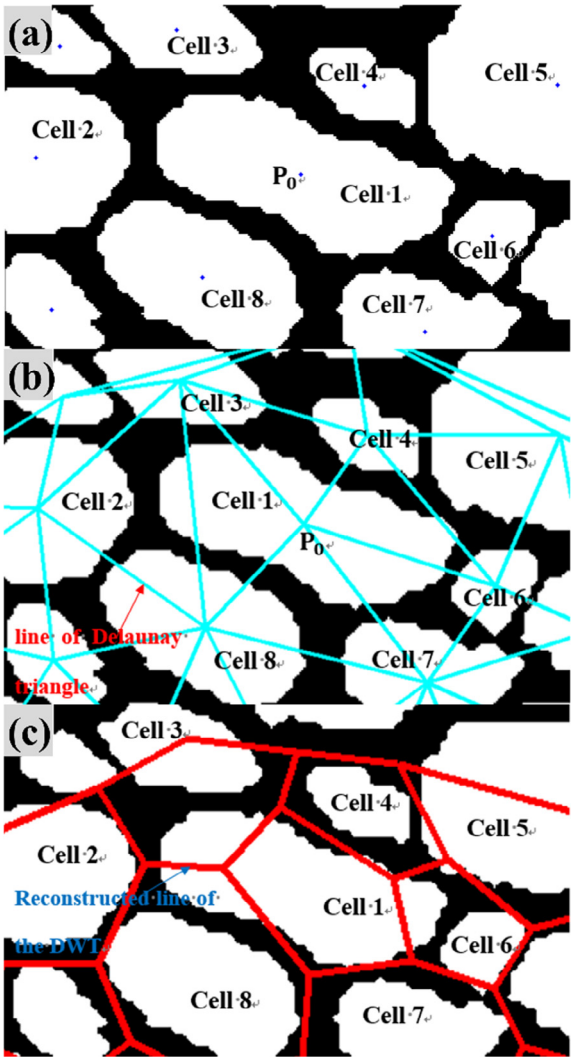


**Fig. 5.** The flowchart of DWT-based Delaunay triangulation: (a) Binary image. $P_0$ is the centroid point of the elongated cell 1, and those from cell 2 to cell 8 are the adjacent cells of cell 1. (b) Delaunay triangulation. The cyan lines are the edges of Delaunay triangle. The centroid point of cell 2 or cell 5 is not the apex of the same triangle with the centroid point of cell 1. (c) Reconstructed structures by DWT. Reconstructed lines are shown in red. The reconstructed cell 1 is neither adjacent to cell 2 nor to cell 5, therefore the reconstructed cell 1 is severely distorted.

(1) Extract the centroid points of all cells (Fig. 6a), and calculate the eccentricity of each cell, where the eccentricity is defined as the one of an ellipse that has the same standard second-order central moment as the cell region, or the ratio of the distance between two ellipse foci and the length of the ellipse long axis.
(2) Choose the cells with eccentricity greater than 0.8, and extract the included angles between cell's long axis and X axis, as well as the length of the long axis. The length and included angles are two parameters to make cell 1 equivalent to an ellipse with the same standard second order moment. Eccentricity 0.8 is taken as a threshold value according to our experience, since cells with eccentricity greater than 0.8 are too long to be accurately rebuilt, such as cell 1.
(3) Equally divide the cell's long axis into 5 segments, and extract the coordinates of the four equal points. In Fig. 6b, the four equal points are $P_1$, $P_2$, $P_3$ and $P_4$.

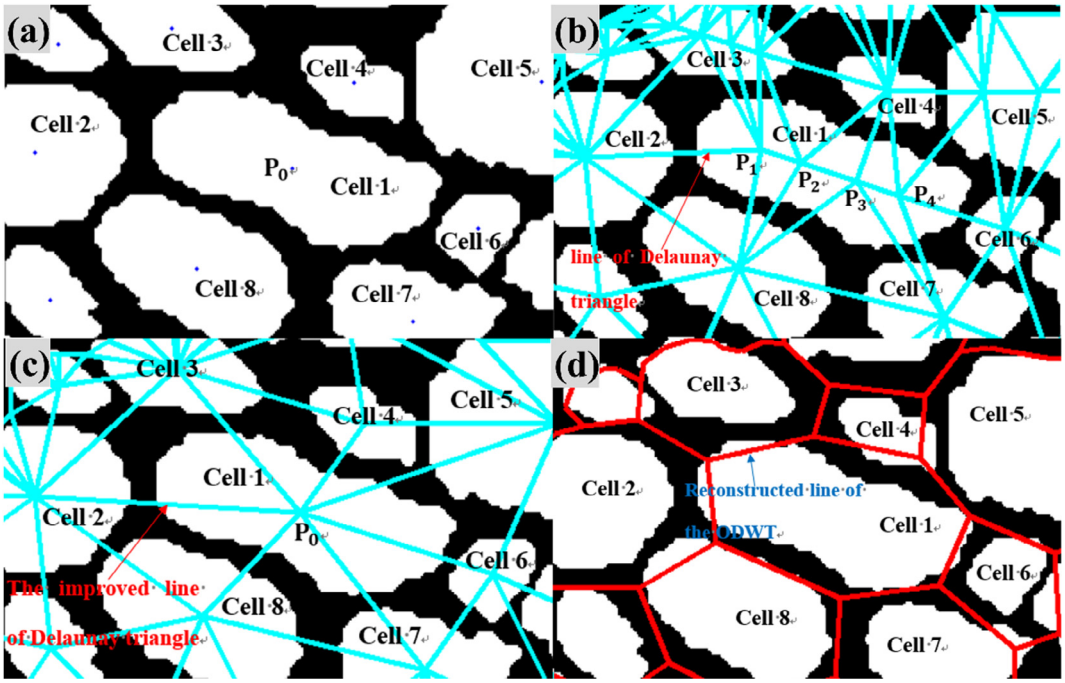


**Fig. 6.** Sequential steps of the DWT-based virtual segmentation (ODWT): (a) Binary image. $P_0$ is the centroid point of the elongated cell 1, and those from cell 2 to cell 8 are the adjacent cells of cell 1. (b) Virtual segmentation. The cyan lines are the edges of Delaunay triangle. $P_1$, $P_2$, $P_3$ and $P_4$ are virtual centroid points. The centroid points of cell 2–8 are respectively in the same Delaunay triangle with at least one of the four points $P_1$, $P_2$, $P_3$ and $P_4$ of cell 1. (c) The improved Delaunay triangulation using virtual segmentation. The centroid points of cell 2–8 are respectively the apexes of the same triangle with $P_0$. (d) Reconstructed structures by ODWT. Reconstructed lines are shown in red. The reconstructed cell 1 is adjacent to those from cell 2 to cell 8. By using ODWT, cell 1 is reconstructed accurately.

(4) Replace the centroid point $P_0$ of cell 1 with the four points $P_1$, $P_2$, $P_3$ and $P_4$. This step is equivalent to the segmentation of cell 1, but not actually segmented. Therefore, the four points $P_1$, $P_2$, $P_3$ and $P_4$ are called virtual centroid points, which can ensure the authenticity of the reconstructed effect. More than four points are of little significance and will increase the computation complexity of the algorithm.
(5) The Delaunay triangulation is operated with the centroid points including $P_1$, $P_2$, $P_3$ and $P_4$. As shown in Fig. 6b, the centroid points of cell 2–8 are respectively in the same Delaunay triangle with at least one of the four points $P_1$, $P_2$, $P_3$ and $P_4$ of cell 1. $P_1$, $P_2$, $P_3$ or $P_4$ are selected and replaced with $P_0$. Then the Delaunay triangulation is changed from Fig. 6b–c.

Based on the optimized triangulation, DWT will achieve realistic segmentation of cell 1 (Fig. 6d). For concave cells, the reconstruction is similar to that of the long cells. Because the distance between the end of the convex region and the centroid of the concave cells is relatively large, the adjacent cells around the convex side cannot be recognized. This phenomenon can also be improved by virtual segmentation.

#### 2.2.3. The finite tissue boundary

For the micrographs of plant tissue with finite tissue boundary contours, CVT is faced with the problem of producing infinite tissue boundaries (Faisal et al., 2012; Ntenga and Beakou, 2011), while AWT fails to reconstruct the outermost cells. To achieve accurate reconstruction of the finite tissue boundary, the binary image is processed using the “closing” operation in MATLAB. In mathematical morphology, the closing operation is defined as a combined operation of first dilation and second erosion. It can be realized by using the “imclose” function in Matlab. Then, the entire tissue section is turned into a large integrated region through operation of erosion and filling in hole, as shown in Fig. 7b. Then the coordinates of the boundary points are obtained using the “bwboundaries” function. For the boundary points, only those points on the boundary with high local curvature are extracted and remained (Fig. 7c), and added to the set of Delaunay triangulation points working as the centroid points of the virtual cells with area value of 1. In the regenerated Delaunay triangle set, the Delaunay triangles whose three apexes are the boundary points are removed. Based on this set of Delaunay triangles, DWT can provide real tissue boundaries. The resulting boundary is fairly consistent with the original boundary, and no manual manipulations or repairing are required. The algorithm could accurately identify the outermost outline of the tissues with finite boundary. For open tissues without the outermost boundary, a straight boundary will be generated, which can be easily removed.

### 2.3. Statistical parameters and evaluating methods

In order to test the effectiveness of the algorithm, the area, eccentricity and edge perimeter of the cells in the reconstructed image were counted and compared with that of the original image, as well as CVT and AWT respectively. These statistical parameters are obtained through the “regionprops” function in Matlab, which is a function used to obtain properties of image region. The cell area is the total number of pixels of each connected region. Eccentricity is defined in Section 2.2. The perimeter is the length of the closed lines connecting the boundary points of each cell zone. Statistical parameters of all cell regions are obtained, and piecewise statistics is made. Parameters, including the mean value, the median value, the quartile and standard deviation of above three geometric parameters concerning both the micrographs and the reconstructed images, were calculated and compared, which are used to make further evaluation to the algorithms. The distributions of the area and eccentricity were imported by Matlab, which makes the comparison more intuitive in a two-dimensional plane.

### 2.4. The 3D shell element model of the plant tissue and the simulation analysis

After the binary image is obtained as shown in Fig. 8a, the 3D shell

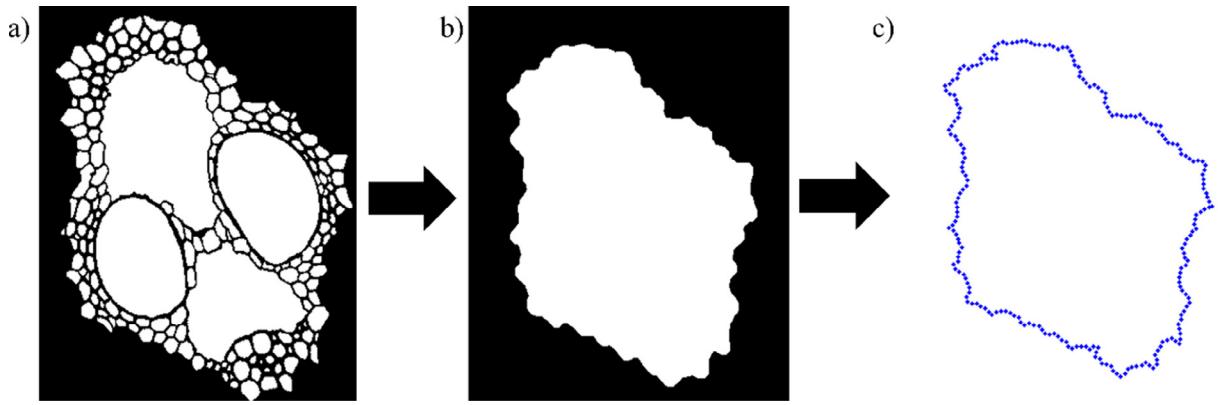


**Fig. 7.** Sequential steps of extracting boundary points of tissue: (a) Microscopic binary image of maize vascular bundle. (Huang et al., 2017, authorized by Springer). (b) A large connected region formed by closed operation. (c) The acquisition of tissue boundary points.

element model can be generated according to the flowchart of Fig. 8. Firstly, the algorithm ODWT was embedded in Matlab to rebuild the structure, shown in Fig. 8b. Then, the reconstructed image was converted into graphic exchange format (DXF) that can be directly imported into the commercial finite element software, for example, ABAQUS (Fig. 8c). The 2D cross section of the plant tissue was extruded along the longitudinal direction in ABAQUS to generate the 3D model (Fig. 8d), which could be applied for finite element analysis. This process is commonly utilized to investigate the mechanical behavior of plant tissue or fibers (Huang et al., 2017; Wang et al., 2014).

By the above process, the CVT, AWT and ODWT algorithms were used to reconstruct the 3D shell model of the retting maize vascular bundle tissue (Fig. 9). Then, the 3D shell models were imported into ABAQUS for simulation analysis and the longitudinal tensile modulus of the model was calculated. In order to compare with the experimental results in reference (Huang et al., 2017), the same material properties of cell wall as in reference (Huang et al., 2017) were used. The vascular bundle fibers were divided into two sections: vessels and phloem tissue (Sv) and vascular bundle sheath (VBS) (Fig. 9d). The cell wall thickness of VBS is 4 μm, the thickness of cell wall in Sv is 1.46 μm. The cell wall material properties and microfibril angle can be found in the reference (Huang et al., 2017).

Static analysis is performed in ABAQUS, considering only elastic deformation. One side of the model is completely fixed and the other side is applied with axial tensile displacement $u$, the longitudinal tensile modulus $E_1$ of the model is calculated by:

$$E_1 = \frac{FL}{Au} \tag{5}$$

where $F$ is the resulting reaction force at fixed side, L is the extrusion length of the model, and S is the cross-sectional area of model.

## 3. Results and discussion

### 3.1. Case study 1 – the reconstructed structures of carrot

As mentioned before, the purpose of the algorithm is to obtain an accurate image that can reflect the real structure of plant tissues so as to

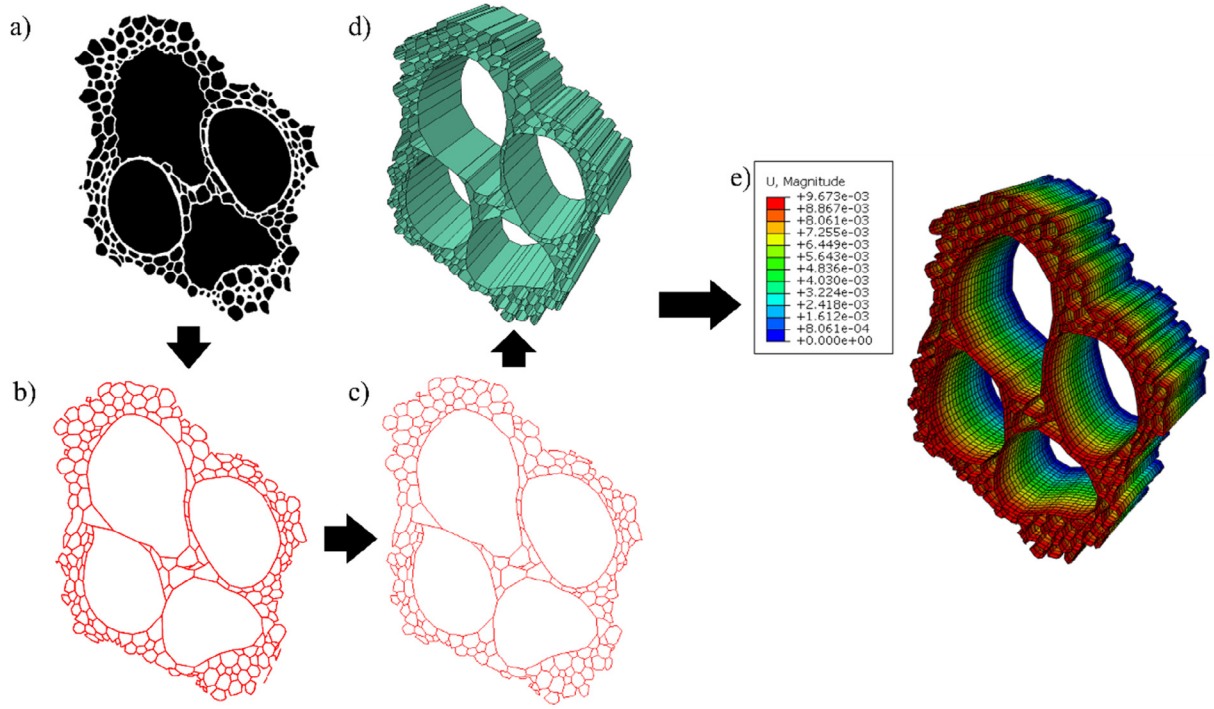


**Fig. 8.** Sequential steps of generating 3D shell element model: (a) the binary image. (From Huang et al. (2017), with permission from Springer.) (b) The reconstructed structure obtained by ODWT. (c) The DXF file. (d) The 3D model. (e) Finite element analysis.

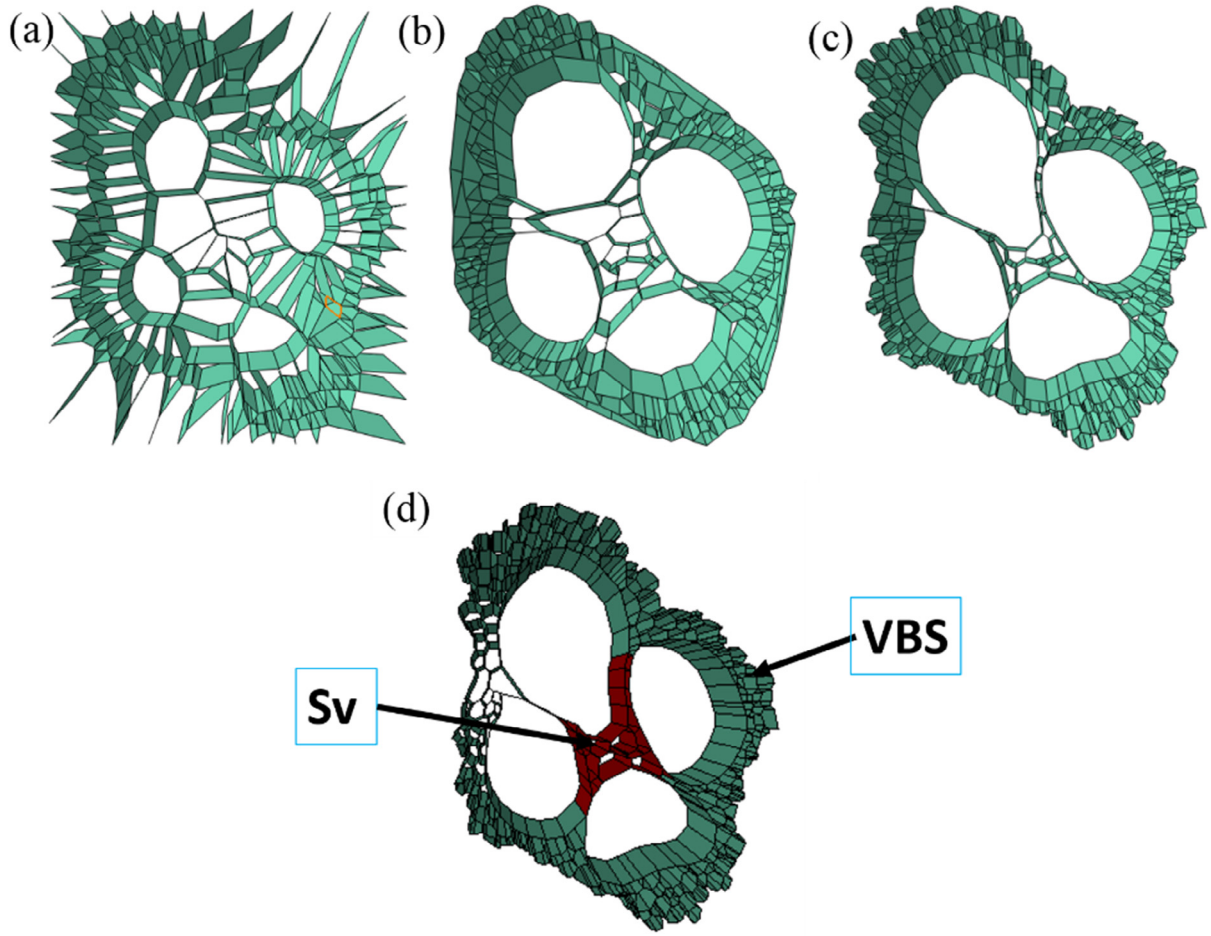


**Fig. 9.** Establishment of 3D shell element model based on three reconstruction algorithms: (a) CVT model. (b) AWT model. (a) ODWT model. (d) Material partitioning of the model. The values of their cell wall thickness in the two sections are different. The cell wall thickness of VBS is thicker than that in Sv.

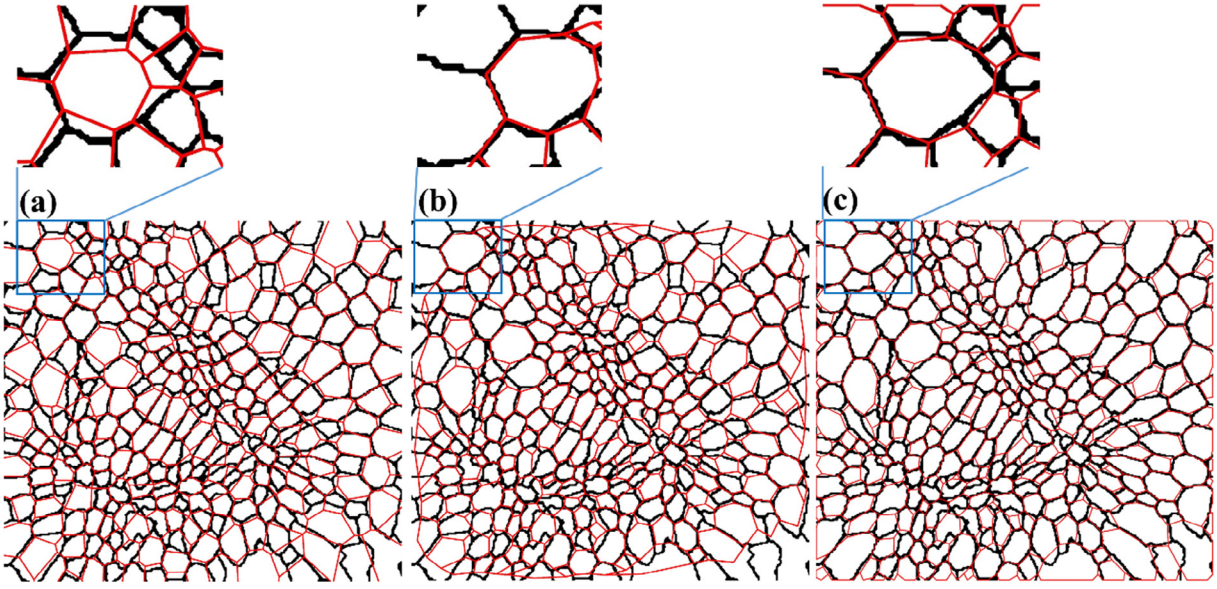


**Fig. 10.** Comparison of carrot tessellation. Reconstructed lines are shown in red. (a) Reconstructed structures using CVT. It smoothens the difference between small cells and big cells. (b) Reconstructed structures using AWT. The reconstruction of tissue boundary is incorrect. (c) Reconstructed structures using ODWT, which provides an accurate reconstruction of the cells.

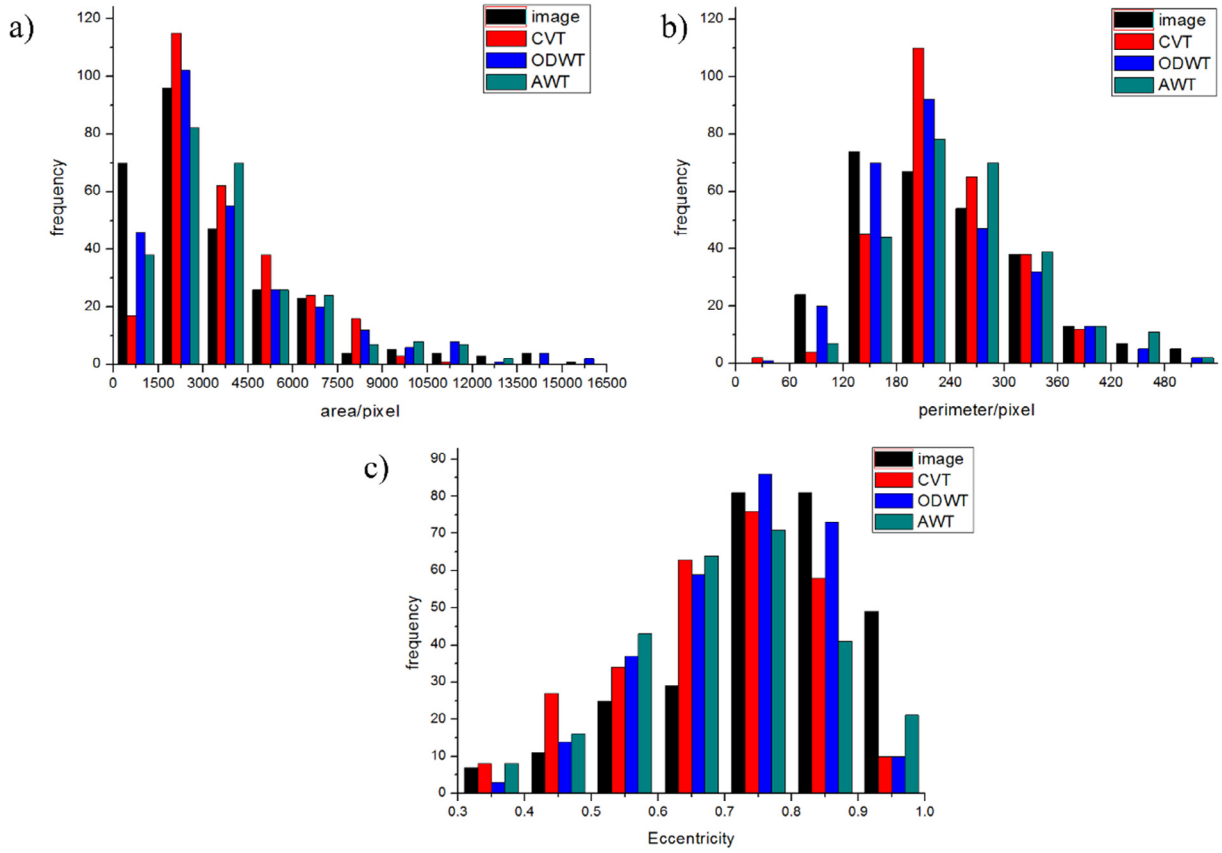


**Fig. 11.** Compared results between the original binary image of carrot and the reconstructed structures of CVT, AWT and ODWT. (a) Area/pixel. (b) Perimeter/pixel. (c) Eccentricity.

increase the simulation accuracy. Therefore, it is necessary to compare the similarity of reconstructed model with the original micrographs. Fig. 10 shows the images of a carrot tissue reconstructed by CVT, AWT and ODWT. As observed from Fig. 3a, the size and shape of carrot cells are diverse. CVT dilutes this diversity. AWT achieves a good reconstruction of the internal structure, but fails to reconstruct cells near the tissue boundary. Remarkably, ODWT almost reproduces the original diversity of cells shape and size.

The statistical comparison of the reconstructed images (Fig. 11) of three methods makes further confirmation that CVT fails to reconstruct cells with severely diverse sizes and shapes. Concerning the area distribution of CVT, it shows that there are quite few cells with area below 1500 or beyond 10,500. Most of cells take the area size between 3000 and 9000. Concerning the perimeter, the number of cells less than 200 or greater than 400 are quite smaller than the real value. Whereas, the number of cells between 200 and 400 are quite bigger than the real value. The distribution of eccentricity is also incorrect. The number of cells with a value less than 0.7 by CVT is very big, which makes the overall eccentricity very small. It implies that the reconstructed carrot tissues tend to become rounder than its initial structure. For AWT, the cells located near the tissue boundary is seriously distorted, and the statistical result is even inferior to CVT for this case. However, ODWT shows obvious advantage in that it tries to restore the huge difference in area and shape between cells, and the statistical result is very close to the original tissue.

As for the mean value of the area and perimeter parameters, the ODWT does not show any advantage over the CVT or AWT, since the total area and number of the cells rebuilt with either ODWT or CVT are basically identical with the original tissues. However, the standard deviation and quartiles of CVT are inaccurate, because it smoothens the difference between small cells and big cells. ODWT is superior to CVT and AWT in the statistics of eccentricity, indicating that ODWT is better in reconstructing the true shape of cellular tissue. Table 1 lists the detailed statistical values of the three methods when reconstructing carrot tissue.

**Table 1**
The statistical results of the carrot's geometric parameters.

| | | Image | CVT | AWT | ODWT |
|---|---|---|---|---|---|
| Mean Value | Area | 3488.4 | 3731.7 | 3814.2 | 3844.2 |
| | Perimeter | 233.9 | 228.7 | 251.3 | 226.4 |
| | Eccentricity | 0.76 | 0.69 | 0.69 | 0.72 |
| Standard deviation | Area | 2936.0 | 2045.4 | 2587.2 | 3092.3 |
| | Perimeter | 97.9 | 63.8 | 83.0 | 84.1 |
| | Eccentricity | 0.15 | 0.15 | 0.14 | 0.13 |
| 1/4 quantile | Area | 1510.0 | 2276.3 | 1951.4 | 1886.1 |
| | Perimeter | 160.4 | 188.1 | 189.8 | 167.4 |
| | Eccentricity | 0.70 | 0.59 | 0.60 | 0.63 |
| Median | Area | 2587.0 | 3111.5 | 3253.9 | 2873.2 |
| | Perimeter | 214.6 | 222.9 | 243.7 | 207.2 |
| | Eccentricity | 0.79 | 0.71 | 0.70 | 0.73 |
| 3/4 quantile | Area | 4443.0 | 4955.0 | 4787.9 | 4819.5 |
| | Perimeter | 290.5 | 279.8 | 299.3 | 274.8 |
| | Eccentricity | 0.87 | 0.79 | 0.80 | 0.82 |

### 3.2. Case study 2 – the reconstruction of retting maize vascular bundle

Different from carrot, retting maize vascular bundles have cells with big difference both in area and in shape. In order to test the adaptive ability of ODWT, the retting maize vascular bundles were chosen as the sample to make a comparison with CVT and AWT.

Fig. 12 shows the images of retting maize vascular bundle

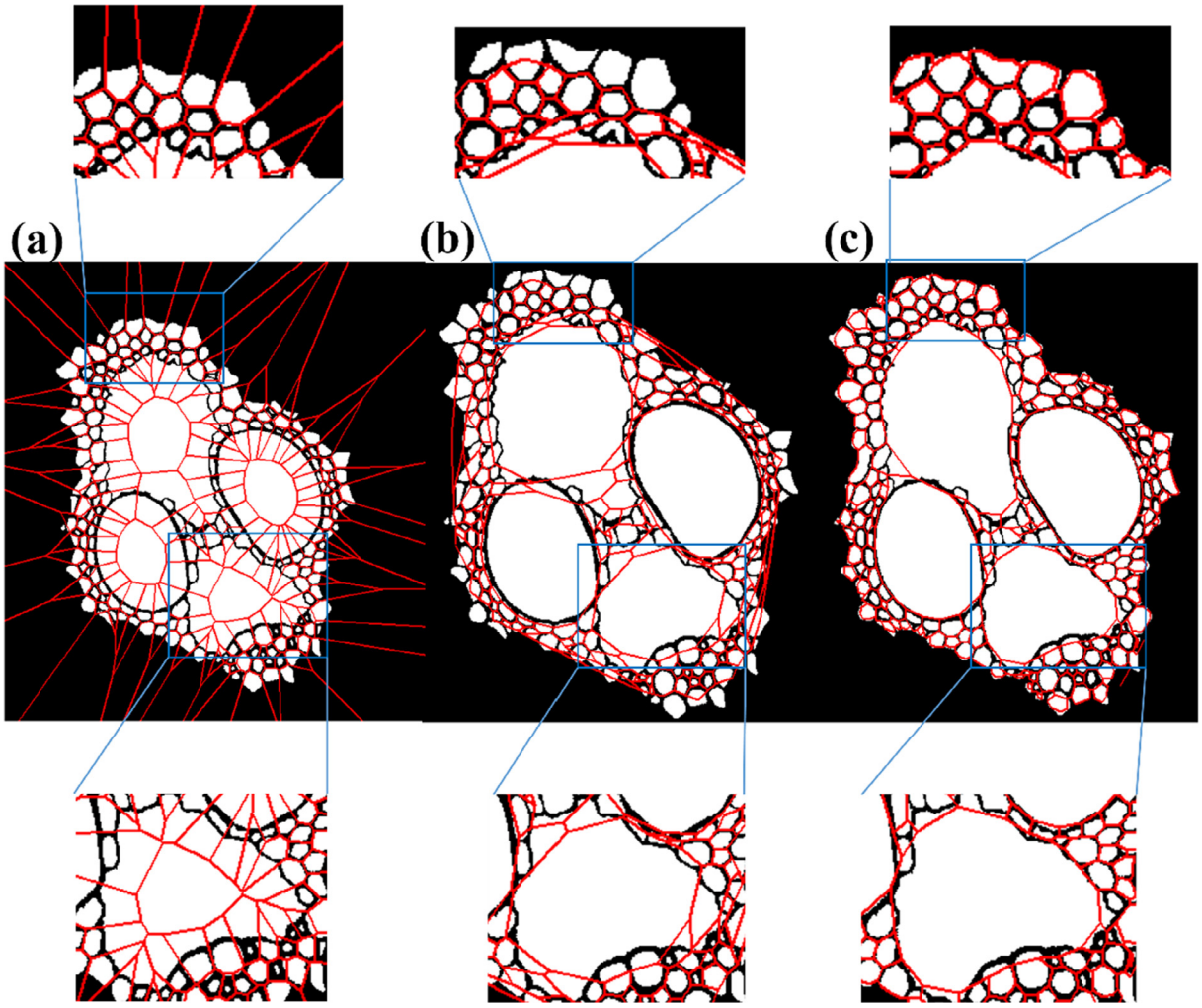


**Fig. 12.** Comparison of retting maize vascular bundle tessellation. Reconstructed lines are shown in red. (a) Reconstructed structures using CVT. Note that the red lines extending to the image boundary and within the large vascular spaces indicate the poor quality of the tessellation. (b) Reconstructed structures using AWT. The concave cavity becomes a convex shape, and the reconstruction of tissue boundary is incorrect. (c) Reconstructed structures using ODWT, which provides a far more accurate reconstruction of the cells.

reconstructed by CVT AWT and ODWT, respectively. In order to intuitively compare the reconstructed results with the original image, the cell structure of the original micrograph is retained on the reconstructed image. The retting maize vascular bundle has four cavities that are much larger than the surrounded cellular zone. CVT has been proven to have defects in that it increases the area of small cells surrounded by large cells and reduces the area of large cells that are surrounded by small cells (Huang et al., 2016; Mebatsion et al., 2006b; Wang et al., 2014). Therefore, it made an obvious change to the shape characteristics of the cells. When the tissue has some extremely large cavities surrounded by small cells, the defects of CVT are intensively exposed. The thin-walled cavities are invaded by the surrounded small cells, which are enlarged and elongated after reconstruction (Fig. 12a). It can be seen that CVT cannot effectively reconstruct the retting maize vascular bundle with large cavity structure surrounded by small cells. AWT manages to make some improvement, but the accuracy is still insufficient. Still, some small cells adjacent to the thin-walled cavity are invaded (Fig. 12b). Based on distance weighted tessellation, the reconstructed line of the ODWT is located exactly at the midline of the adjacent cellular gap, showing the highest reconstruction accuracy (Fig. 12c). Long-shaped cells and concave cavities often appear in retting vascular bundles, which cannot be accurately reconstructed with CVT and AWT, where the long-shaped cells become shorter and square, and the concave cavity becomes a convex shape.

Based on virtual segmentation, ODWT has achieved a well-reconstructed morphological characteristics of these two structures, including long cells and concave polygons. Through this case study, it is proven again that ODWT is especially effective in reconstructing tissues with complex structures like irregular cell shape and non-uniform cell size. In contrast, CVT is incapable of processing finite boundary, and manual repairing is needed to obtain a finite tissue boundary. As for AWT, it could not directly obtain the tissue boundary of the outermost cell. The case study of the retting maize vascular bundle shows that the concave boundary is seriously distorted, and turned from concave into convex. However, the ODWT shows the advantage in tissue boundary identification. What deserves to be mentioned is that no repair is demanded after reconstruction.

In order to carry out a quantitative analysis of the three algorithms, the statistic values are also calculated and compared. Fig. 13 shows the comparison of statistical results from the original micrographs and the images reconstructed by CVT, AWT and ODWT. When the area is greater than 8000 or the perimeter is greater than 400 or the eccentricity is greater than 0.9, the number of cells in the AWT and CVT is abnormally increased. For AWT, the concave-shaped cavities and their adjacent cells cannot be accurately rebuilt, as well as the tissue boundary distortion. For CVT, severe distortion happened during the reconstruction of the four large cavities and their adjacent cells. However, ODWT performs the best concerning all statistical parameters,

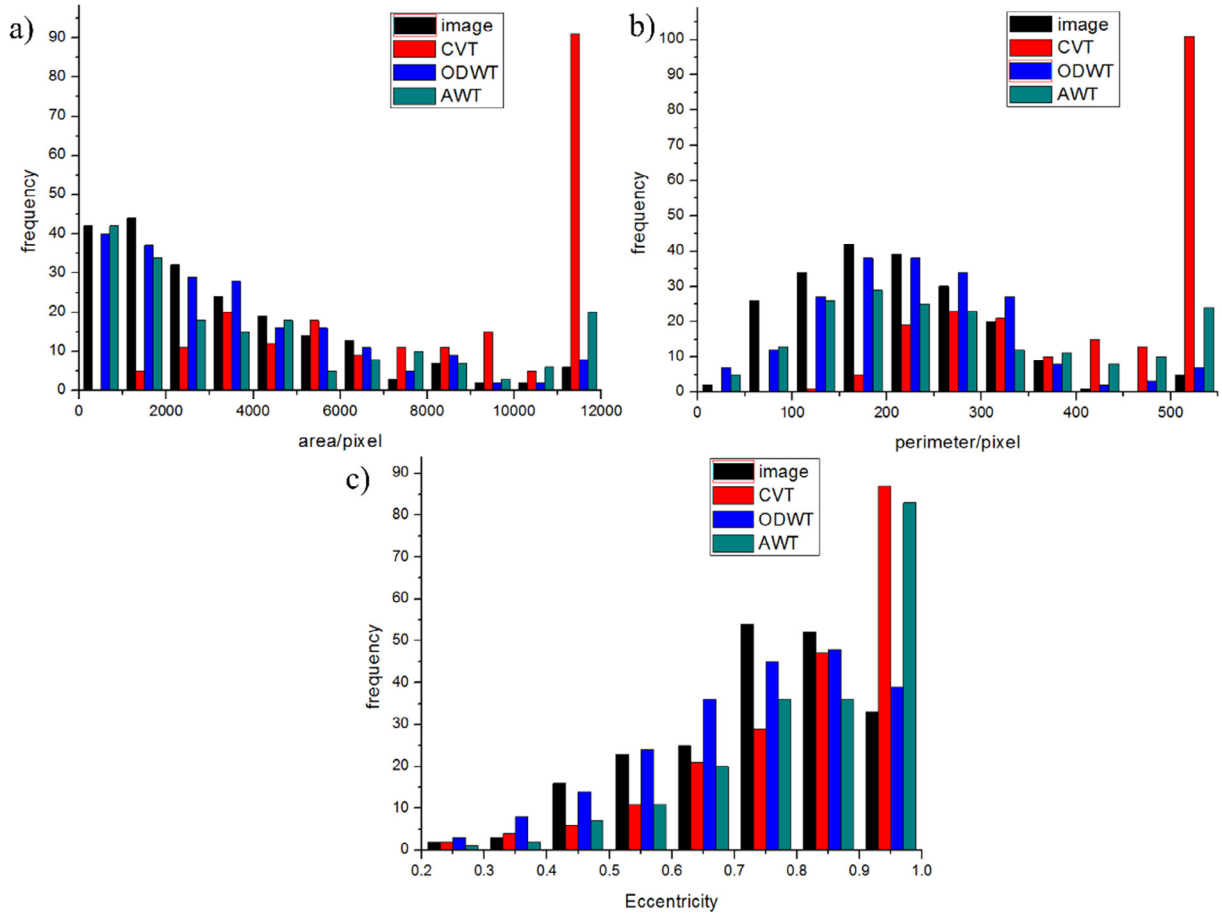


**Fig. 13.** Compared results between the original binary image of maize vascular bundle tissue and the reconstructed structures of CVT, AWT and ODWT. (a) Area/pixel. (b) Perimeter/pixel. (c) Eccentricity.

**Table 2**
The statistical results of the maize vascular bundle tissue's geometric parameters.

| | | Image | CVT | AWT | ODWT |
|---|---|---|---|---|---|
| Mean Value | Area | 9187.9 | 16415.3 | 12262.1 | 10977.5 |
| | Perimeter | 244.4 | 529.6 | 295.1 | 261.1 |
| | Eccentricity | 0.74 | 0.81 | 0.82 | 0.72 |
| Standard deviation | Area | 44846.9 | 21456.8 | 62837.5 | 56382.2 |
| | Perimeter | 318.9 | 274.3 | 368.7 | 324.7 |
| | Eccentricity | 0.16 | 0.16 | 0.16 | 0.17 |
| 1/4 quantile | Area | 1134.5 | 5167.3 | 1075.4 | 1236.3 |
| | Perimeter | 135.8 | 314.9 | 154.5 | 161.6 |
| | Eccentricity | 0.65 | 0.71 | 0.72 | 0.61 |
| Median | Area | 2596.5 | 9491.8 | 2943.1 | 2845.0 |
| | Perimeter | 200.8 | 487.9 | 243.0 | 216.0 |
| | Eccentricity | 0.76 | 0.87 | 0.88 | 0.75 |
| 3/4 quantile | Area | 4642.0 | 18145.8 | 6956.0 | 5152.3 |
| | Perimeter | 266.9 | 632.9 | 382.6 | 287.3 |
| | Eccentricity | 0.86 | 0.93 | 0.95 | 0.86 |

which are quite close to the statistical results of the original microscopic images.

All the statistics parameters related to the image authenticity are shown in Table 2. It is obvious that most of the parameters of CVT deviate significantly from that of the original image. The mean values of area and perimeter parameters of AWT are much larger than that of ODWT, because some small cells adjacent to the thin-walled cavity are invaded and disappear during reconstruction. In addition, AWT cannot reconstruct the cells near the tissue boundary, which leads to the cell loss during reconstruction. The standard deviation, the quartiles and the eccentricity of the reconstructed image from ODWT are quite close to the original micrograph, indicating that the reconstructed structure successfully inherits the authenticity of the original micrograph.

Figs. 14 and 15 are contours of the distribution of area and eccentricity. It is meaningful to visually show the location of the cells with different sizes and eccentricity in the reconstructed images. Thus, it can reflect the reconstruction effect of ODWT and AWT in the two-dimensional space. In contrast to AWT, the reconstructed image of ODWT is significantly similar to the original micrograph when comparing the distribution of cell area and eccentricity. The morphological features of most cells are truly reproduced. Although the reconstructed image by AWT is not much different from the microscopic image in the overall distribution, the area of cells adjacent to the two concave cavities is greatly deviated from the original micrograph. The area distribution near tissue boundaries is also unsatisfactory. In the meanwhile, the reconstructed image of AWT is less effective than that of the ODWT in the distribution of eccentricity, and it is not similar enough to the initial micrograph on the overall distribution of the cell eccentricity.

Table 3 compared the simulated values of the longitudinal tensile modulus of three models with the experimental value. The relative error of the values of CVT model is the largest, which cannot accurately predict the longitudinal elastic modulus of the retting maize vascular bundle. The simulated values of the ODWT model are the closest to the experimental values, and the relative error is 6.812%. The comparison results show that the reconstruction algorithms have great influence on the prediction accuracy of the mechanical properties of multi-scale models. The accurate reconstruction of plant tissue by ODWT algorithm

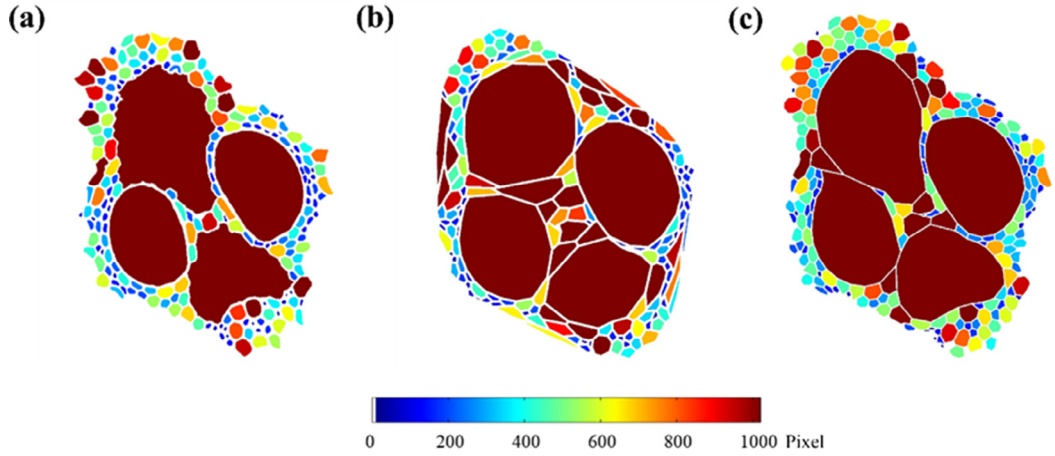


**Fig. 14.** The contours of the area distribution of (a) the original binary image. There are many small cells around the four large cavities. (b) AWT. The area of cells adjacent to the two concave cavities is greatly deviated from the original micrograph. (c) ODWT. The reconstructed image by ODWT is similar to the micrograph in the distribution of cell area.

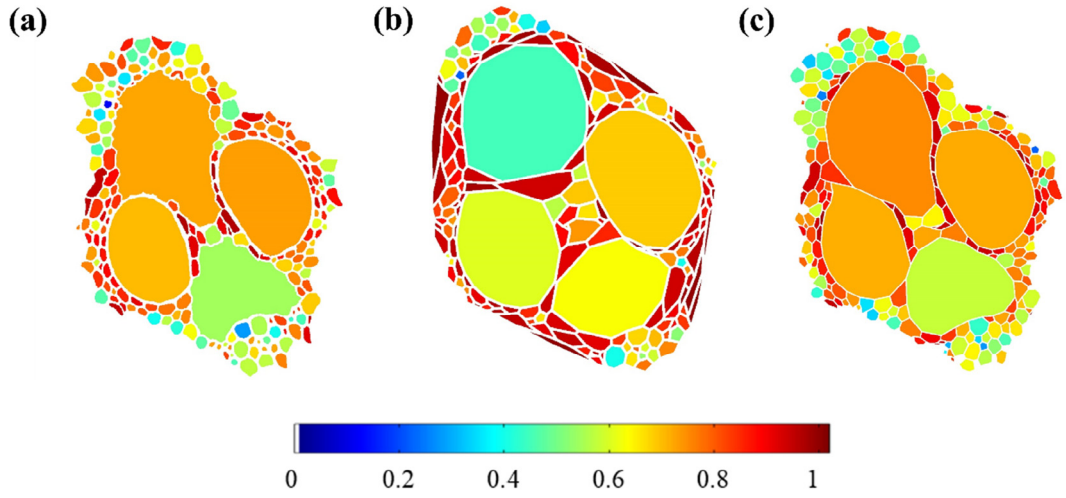


**Fig. 15.** The contours of the eccentricity distribution of (a) the original binary image. (b) AWT. The eccentricity of the two concave cavities is greatly deviated from the original micrograph. Many elongated cells are generated at the boundary. (c) ODWT. The reconstructed image by ODWT is similar to the micrograph in the distribution of cell eccentricity.

**Table 3**
The simulated values of the longitudinal elastic modulus of three models and the experimental value.

| – | Elastic modulus (GPa) | Relative error (%) |
|---|---|---|
| Experimental value | 12.463 | – |
| CVT model | 17.864 | 43.336 |
| AWT model | 15.644 | 25.524 |
| ODWT model | 13.312 | 6.812 |

can effectively improve the prediction accuracy of multi-scale models on mechanical properties.

## 4. Conclusion

The purpose of this work is to develop an algorithm that can accurately reconstruct the structures of plant tissues. The reconstructed model can be directly imported into the numerical software for further analysis without preprocessing. A technique of virtual segmentation was developed to optimize the Delaunay triangulation. Based on the optimized Delaunay triangulation, an optimized distance weighted tessellation algorithm with finite tissue boundary was developed. The accuracy of ODWT was verified by taking two different plant structures as examples, and compared with that of the CVT and AWT algorithms. Through statistical analysis of various geometrical parameters, the accuracy of ODWT in reconstructing plant tissues was further confirmed. When the cell shape is elongated, concave or the area of adjacent cell is quite different, ODWT has obvious advantages over the CVT and the AWT. This algorithm was developed to fulfill the reconstruction of the mechanical model of the plant tissue with higher accuracy so as to make sure that the simulation analysis of the mechanical properties of the plant tissue can be performed more effectively. The comparison results of the simulated values of the longitudinal tensile modulus with the experimental value show that ODWT algorithm can improve the prediction accuracy of multi-scale models on mechanical properties.

## Declaration of Competing Interest

The authors declare that they have no known competing financial interests or personal relationships that could have appeared to influence the work reported in this paper.

## Acknowledgements

The authors gratefully acknowledge the financial support from the National Natural Science Foundation of China (No. 11572128), Natural Science Foundation of Guangdong Province, China (No. 2016A030311052) and China Postdoctoral Science Foundation (No. 2019TQ0180).

## References

Andronov, L., Michalon, J., Ouararhni, K., Orlov, I., Hamiche, A., Vonesch, J.L., Klaholz, B.P., 2018. 3DClusterViSu: 3D clustering analysis of super-resolution microscopy data by 3D Voronoi tessellations. Bioinformatics 34, 3004–3012.

Faisal, T., Rey, A., Pasini, D., 2013. A multiscale mechanical model for plant tissue stiffness. Polymers 5, 730–750.

Faisal, T.R., Hristozov, N., Rey, A.D., Western, T.L., Pasini, D., 2012. Experimental determination of Philodendron melinonii and Arabidopsis thaliana tissue microstructure and geometric modeling via finite-edge centroidal Voronoi tessellation. Phys. Rev. E 86, 031921.

Faisal, T.R., Hristozov, N., Western, T.L., Rey, A.D., Pasini, D., 2014. Computational study of the elastic properties of Rheum rhabarbarum tissues via surrogate models of tissue geometry. J. Struct. Biol. 185, 285–294.

Ghosh, S., Lee, K., Moorthy, S., 1996. Two scale analysis of heterogeneous elastic-plastic materials with asymptotic homogenization and Voronoi cell finite element model. Computer Methods Appl. Mech. Eng. 132, 63–116.

Gibson, L.J., 2005. Biomechanics of cellular solids. J. Biomech. 38, 377–399.

Huang, J., Liu, W., Zhou, F., Peng, Y., 2017. Stiffness variability analysis of maize fiber bundles via multiscale simulation. J. Mater. Sci. 52, 7917–7928.

Huang, J., Liu, W., Zhou, F., Peng, Y., Wang, N., 2016. Mechanical properties of maize fibre bundles and their contribution to lodging resistance. Biosyst. Eng. 151, 298–307.

Jin, K., Qin, Z., Buehler, M.J., 2015. Molecular deformation mechanisms of the wood cell wall material. J. Mech. Behav. Biomed. Mater. 42, 198–206.

Lee, D.T., Schachter, B.J., 1980. Two algorithms for constructing a Delaunay triangulation. Int. J. Comput. Inf. Sci. 9, 219–242.

Liu, W., Huang, J., Wang, N., Lei, S., 2015. The influence of moisture content on the interfacial properties of natural palm fiber–matrix composite. Wood Sci. Technol. 49, 371–387.

Luo, Y., Samwer, K., 2018. Local atomic order of a metallic glass made visible by scanning tunneling microscopy. J. Phys. Condens. Matter 30, 245702.

Malek, S., Gibson, L.J., 2017. Multi-scale modelling of elastic properties of balsa. Int. J. Solids Struct. 113–114, 118–131.

Malek, S., Raney, J.R., Lewis, J.A., Gibson, L.J., 2017. Lightweight 3D cellular composites inspired by balsa. Bioinspir. Biomimetics 12, 026014.

Mattea, M., Urbicain, M.J., Rotstein, E., 1989. Computer model of shrinkage and deformation of cellular tissue during dehydration. Chem. Eng. Sci. 44, 2853–2859.

Mebatsion, H.K., Verboven, P., Verlinden, B.E., Ho, Q.T., Nguyen, T.A., Nicolaï, B.M., 2006a. Microscale modelling of fruit tissue using Voronoi tessellations. Comput. Electron. Agric. 52, 36–48.

Mebatsion, H.K., Verboven, P., Ho, Q.T., Verlinden, B.E., Mendoza, F., Nguyen, T.A., Nicolaï, B.M., 2006b. Modeling Fruit Microstructure Using an Ellipse Tessellation Algorithm.

Ntenga, R., Beakou, A., 2011. Structure, morphology and mechanical properties of Rhectophyllum camerunense (RC) plant-fiber. Part I: Statistical description and image-based reconstruction of the cross-section. Comput. Mater. Sci. 50, 1442–1449.

Palombini, F.L., Kindlein, W., de Oliveira, B.F., de Araujo Mariath, J.E., 2016. Bionics and design: 3D microstructural characterization and numerical analysis of bamboo based on X-ray microtomography. Mater. Charact. 120, 357–368.

Pieczywek, P.M., Zdunek, A., Umeda, M., 2011. Study on parameterisation of plant tissue microstructure by confocal microscopy for finite elements modelling. Comput. Electron. Agric. 78, 98–105.

Rafsanjani, A., Derome, D., Wittel, F.K., Carmeliet, J., 2012. Computational up-scaling of anisotropic swelling and mechanical behavior of hierarchical cellular materials. Compos. Sci. Technol. 72, 744–751.

Saavedra Flores, E.I., Haldar, S., 2016. Micro–macro mechanical relations in Palmetto wood by numerical homogenisation. Compos. Struct. 154, 1–10.

Wang, N., Liu, W., Lai, J., 2013. An attempt to model the influence of gradual transition between cell wall layers on cell wall hygroelastic properties. J. Mater. Sci. 49, 1984–1993.

Wang, N., Liu, W., Huang, J., Ma, K., 2014. The structure-mechanical relationship of palm vascular tissue. J. Mech. Behav. Biomed. Mater. 36, 1–11.

Zdunek, A., Umeda, M., 2005. Influence of cell size and cell wall volume fraction on failure properties of potato and carrot tissue. J. Texture Stud. 36, 25–43.